Article

Polarized-Electrochemiluminescence Biosensor Based on Surface Plasmon Coupling Strategy and Fluorine-doped BN Quantum Dots

Zihui Liang, Qian Zhang, Yixin Nie, Xin Zhang, and Qiang Ma

Anal. Chem., **Just Accepted Manuscript** • DOI: 10.1021/acs.analchem.0c01558 • Publication Date (Web): 15 Jun 2020

Polarized-Electrochemiluminescence Biosensor Based on Surface Plasmon Coupling Strategy and Fluorine-doped BN Quantum Dots

Zihui Liang, Qian Zhang, Yixin Nie, Xin Zhang and Qiang Ma*

Department of Analytical Chemistry, College of Chemistry, Jilin University, Changchun, 130012,China

* E-mail: qma@jlu.edu.cn

ABSTRACT: The first polarized-electrochemiluminescence (ECL) biosensor is reported in this work. Surface plasmon coupling ECL (SPC-ECL) strategy is developed for the amplified polarization light of fluorine-doped BN Quantum Dot (F-BN QD) emitters. The generation of polarized-ECL is attributed to the characteristic of polarization-angle-dependent SPC effect. A polarized sandwich-type biosensor based on F-BN QDs and Au Nanoparticles (Au NPs) is established to detect K-ras gene. The polarized-ECL sensor is more sensitive with lower detection limit than isotropic ECL sensing system. The sensor can quantify K-ras gene from 0.1 fM to 10 nM with the detection limit as 0.03 fM. This work not only explores polarized SPC-ECL, but also offers a new analytical method for clinical diagnosisn. The generation of polarized-ECL and the amplification strategy of SPC effect open a new path for ECL resolved analysis.

Electrochemiluminescence (ECL) is characterized by high sensitivity, fast response speed, wide dynamic range and simple instrumentation. The process of ECL is that excited state produced by electron transfer relaxes accompanied by luminescence to the ground state. ECL has unique advantages over other luminescence methods. ECL does not need additional excitation source, which overcomes the limitation of background interference (such as autofluorescence and scattered light). The luminophore can recycle with labile active intermediates generated on-site in ECL reaction. Furthermore, the light generated by ECL improves reaction controllability of temporal and spatial. Therefore, ECL becomes a very powerful analytical technique in the sensing research and commercial clinical applications.[1-4] Since QDs ECL was reported in 2002, many QDs (including chalcogenide QDs,[5] carbon nanodots,[6] graphene QDs[7] and so on) have been utilized in the ECL system.[8-10] Compared with traditional ECL luminophores, QDs possess some advantages of ideal optical properties and flexible modification methods. The ECL properties of QDs can be regulated by heteroatom doping and nanostructure tailoring. Meanwhile, various functional nanoparticles (NPs) (e.g. metal NPs and magnetic NPs) and sensing strategies (e.g. ECL-RET and surface enhanced ECL) contribute to expanding the exploration of QD-based ECL systems. Nowadays, the current trends in ECL analysis are high-throughput sensing and real-time dynamic detection.[11-14]

In order to improve ECL sensing capabilities with high sensitivity and high resolution, it needs in-depth information from the obtained luminescence signals. Until now, almost high resolution ECL sensing strategies are based on the wavelength-resolved spectrum information.[15,16] ECL luminophores with different emission peaks are employed in the wavelength-resolved ECL system. For example, multiplex ECL analysis and ratiometric ECL detection have been constructed with the wavelength-resolved mode.[17-19] The luminescence intensities at different wavelength are separated and recorded, respectively. There are some limitations in the wavelength-resolved sensor, such as spectra overlap of the ECL luminophores, low wavelength resolution, and signal interference from the coreactant. Therefore, the exploration for more optical information is an interesting topic in ECL sensing. Polarized luminescence with good specific response and ultralow background interference has significant research potential in high resolution sensing system. Lacour and Sojic have reported that the ECL circular polarization can be produced from the organic derivative.[20] However, because less luminophores have polarized ECL response, it is hard to construct selective polarized ECL sensor for bioanalysis except chiral detection. To date, the sensing system based on polarized-ECL has not been reported.

In this work, we developed a novel polarized-ECL biosensor based on SPC-ECL strategy. SPC-ECL is a kind of unique ECL signals amplification strategy.[21] Due to the resonance interaction of the incident light (as ECL signals) with electron oscillation in the noble metal (such as Au NPs), the coupling of light emission and surface plasmon can result in the luminescence signal amplication. More importantly, SPC-ECL possess the characteristic of polarized angle-dependence. The coupled energy can be radiated into the substrate at a defined angle on account of the polarized angle-dependent SPC effect of Au NPs.[22] Based on the concept of SPC-ECL, the isotropic ECL of most luminophores could be amplified and changed to polarized light. In order to provide stable and modifiable ECL signals, F-doped BN QDs were prepared as ECL luminophores. The strong electron absorption capacity of F atom reduced the energy gap between the singlet states, which can improve the ECL intensity and enhance the luminous stability

Scheme 1. (A) Polarized SPC-ECL Mechanism of F-BN QDs; (B) Schematic Illustration of Polarized ECL Sensor.

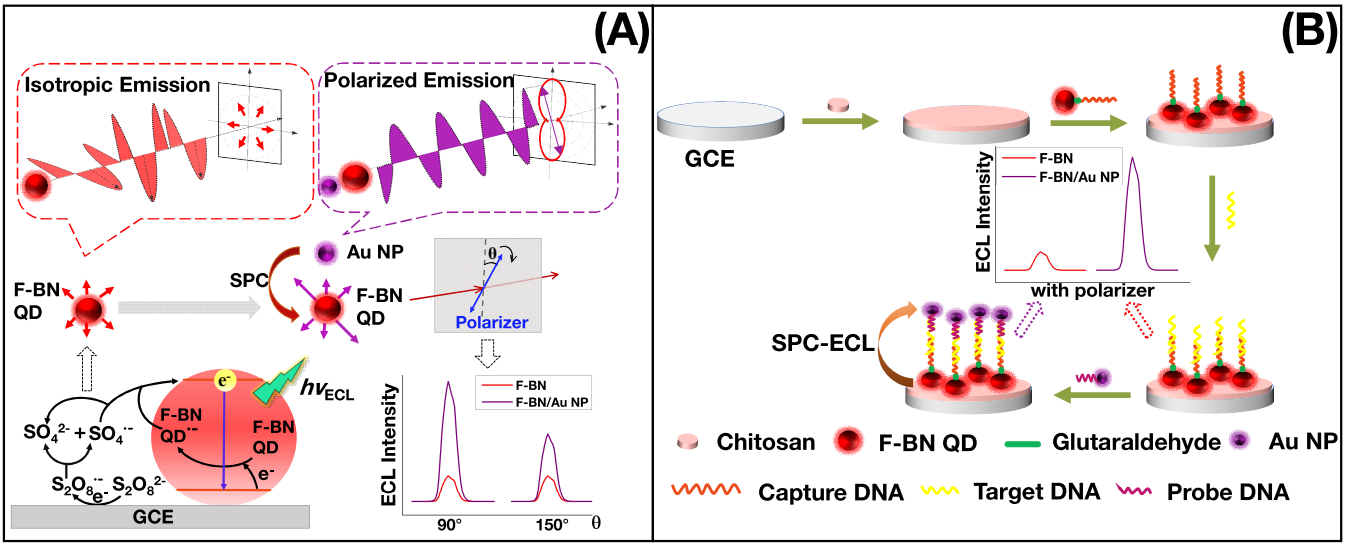

of QDs. As a result, the isotropic ECL emission of F-BN QDs can be amplified to varying degree due to the SPC effect (Schematic 1A). The polarized ECL can be detected with the assistance of a polarizer.

EXPERIMENTAL SECTION

Synthesis of F-BN QDs. F-BN QDs were synthesized by microwave-assisted hydrothermal synthesis pathway. H_3BO_3 (1.6 mmol), $C_3H_6N_6$ (0.27 mmol) and NH_4F were dissolved in 10 mL of ultrapure water. In synthesis of F-BN QDs, the different amounts of NH_4F (1.9 mmol, 2.5 mmol, 3 mmol, 5 mmol and 8 mmol) were used. The reaction was performed for 60 minutes at microwave frequency of 1000 Hz and at 180 ºC. After reaction completed, the solution was cooled to get flocculent precipitated mixture. The F-BN QDs product was centrifuged at 5000 rpm for 10 minutes to remove excess precursor.

Preparation of F-BN QD-GA-Capture DNA. First, 1 mL of F-BN QDs was reacted with 100 μL of 2% Glutaraldehyde (GA) in the dark for 1 h. Then, 100 μL of 10 μM Capture DNA was added into the mixture solution. After 2 h incubation, F-BN QDs-GA-Capture DNA biocomposite can be parpared. The above solution was dialyzed through dialysis membrane (1 KDa) for 4 h to remove unreacted DNA. The obtained solution was stored at 4 ºC until use.

Preparation of Probe DNA-Au NP. Au NPs were prepared according to citrate reduction method. 0.50 mL of 1% $Na_3C_6H_5O_7{\cdot}2H_2O$ was added into 50 mL of 0.01% $HAuCl_4$. After heating, Au NPs were successfully prepared when the color of solution changed from yellow to purple. Au NPs solution was stored at 4 ºC. 30 μL of 1 mg/mL EDC and 30 μL of 0.5 mg/mL NHS were dropped to 1 mL of Au NPs for 0.5 h to activate Au NPs carboxyl group.[23] Then, 100 μL of 10 μM Probe DNA was added to the above solution. After incubated for 2 h, Probe DNA-Au NPs was prepared. To remove unreacted DNA, the above product was dialyzed through dialysis membrane (1 kDa) for 4 h. The resulting Probe DNA-Au NPs solution was stored at 4 ºC.

Polarized ECL detection. Prior to ECL measurement, GCE was polished by α-Al_2O_3 powder and ultrasonically cleaned with ethanol and ultrapure water. The ECL signal was collected by Hamamatsu CR125 photomultiplier tube. The isotropic ECL data was recorded without polarizer. In order to detect polarized ECL signal, a polarizer was fixed between PMT and sample chamber. The ECL intensities of system were acquired when polarizer angles(θ) at 0°, 30°, 60°, 90°, 120°, 150°, 180°, 210°, 240°, 270°, 300° and 330°. For the K-ras gene detection, the electrode was immersed in a 0.2 wt% chitosan aqueous solution for 5 minutes to bind F-BN QDs. Then, 6 μL F-BN QD-GA-Capture DNA was dropped on the above electrode. The non-specific binding sites were blocked by 200 μL of 0.01 wt% bovine serum albumin. The modified working electrode was incubated with 200 μL of different concentrations of K-ras gene at 66 ºC for 6 minutes. The electrode was washed with ultrapure water to release uncaptured target DNA. In the next step, the above electrode was incubated with 200 μL of Probe DNA-Au NPs at 66 ºC for 6 min. The sensing system was cooled to room temperature and washed by ultrapure water to remove excessive reagent. The ECL detection was performed in PBS (pH=7.4) containing 0.1M $K_2S_2O_8$. The working voltage was 0 ~ -2.5V. Scan rate was 0.1V/S. EIS was measured in 0.1 mol/L KCl solution containing 2.5mmol/L $K_3[Fe(CN)_6]/K_4[Fe(CN)_6]$. The impedance spectra were recorded in the frequency range of 0.01 Hz to 100 kHz with an amplitude of 5 mV.

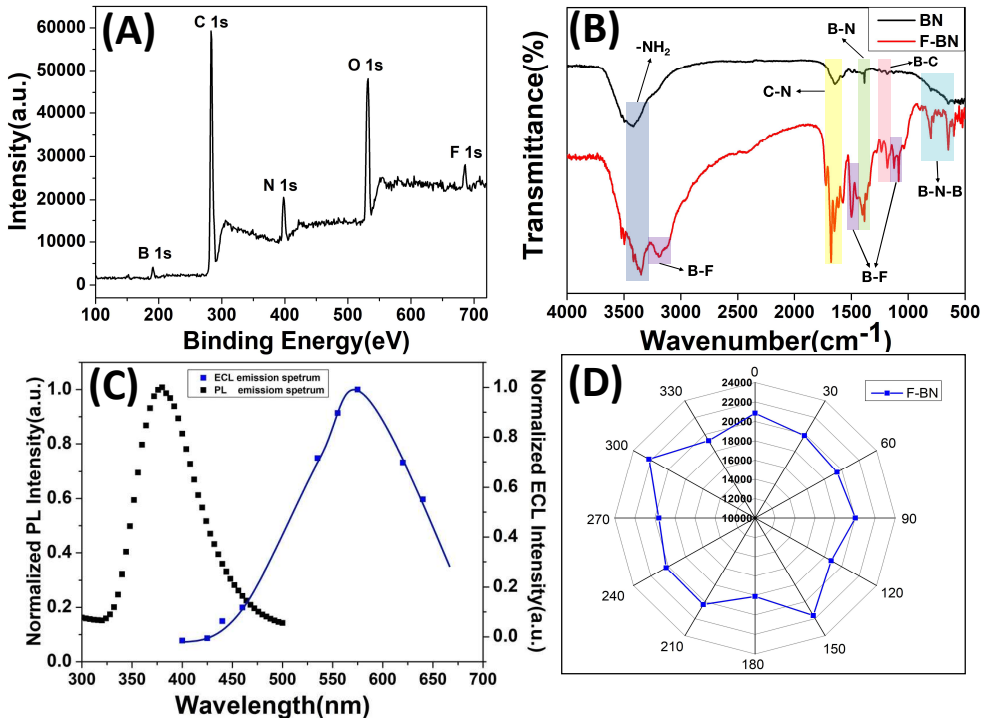

Figure 1. (A) XPS survey spectra of F-BN QDs. (B) FT-IR spectrum of BN QDs and F-BN QDs. (C) ECL spectrum and PL spectrum of F-BN QDs. (D) Radar chart of ECL intensity of F-BN QDs at different polarization angle.

RESULT AND DISCUSSION

The morphology of F-BN QDs was characterized by TEM. As seen in Figure S1, F-BN QDs had a diameter of 2-3 nm with clearly ordered lattice fringes. The composition and property of F-BN QDs were characterized next. The XPS spectrums of F-BN QDs were shown in Figure 1A and Figure S2. It can be seen from Figure 1A that five main peaks at 191.5 eV, 285.9 eV, 399.5 eV, 533.7 eV and 687.0 ev corresponded to B, C, N, O and F of F-BN QDs, respectively. Compared with B and N element, F element is a highly negative charged element and has excessive number of valence electrons. The doped F atom tended to replace N atom in BN QDs. F 1s peak signal in the XPS spectrum was located at 687.0 eV, which can be associated with the B atom in the B-N-B bond.[24,25] It indicated that F atoms were covalently modified with some B atoms on the surface of BN QDs. In the XPS spectrum of B 1s (Figure S2A), the curve-fitted spectrum of B 1s core level electrons showed the B-N bond and the presence of weak sp^3-hybridized B-F bond.[26] The FT-IR spectrum of BN QDs and F-BN QDs were shown in Figure 1B. The result indicated that 636 cm^{-1} and 1375 cm^{-1} corresponded to B-N-B out-of-plane bending vibration and B-N in-plane tensile vibration, respectively. The peak at 1100 cm^{-1} was attributed to the C-B stretching vibration. 3430 cm^{-1} peak corresponded to -NH_2. And the C-N extension peak appeared at 1638 cm^{-1}.[27] Compared to BN QDs, F-BN QDs showed the primary vibrational features of the covalent B-F bonds at approximately 1235 cm^{-1}, 1521.3 cm^{-1} and 3142.0 cm^{-1}.[28] These results were in good agreement with XPS data and clearly indicated the presence of F-BN QDs by covalent functionalization. The UV-vis spectrum of BN QDs (Figure S3) showed that the absorption peak was concentrated at 235 nm, which was attributed to the π-π * electron transition. A significant feature of BN QDs was the wide band gap.[29] The strong electron absorption effect of F atom changed the energy level of F-BN QDs. The energy gap was reduced and the influence of the π–π * conversion was weakened. As a result, the absorption band became wide and the peak value decreased. The band gaps of F-BN and BN QDs can be calculated to be 4.70 eV and 4.90 eV, respectively.

Figure 1C and S4 showed the PL and ECL spectra of F-BN QDs and BN QDs, respectively. The ECL behavior was depended on the surface state and functional groups at a large extent. The difference in the ECL spectra wavelength of two kind QDs indicated that F atoms were doped into F-BN QDs. Due to the strong electron withdrawing characteristic of fluorine, the band gap of F-BN QDs became narrowed. Therefore, the ECL emission peak of F-BN QDs red-shifted to 575 nm compared with BN QDs at 555 nm. It was in agreement with the narrow band gap of F-BN QDs (4.70 eV) corresponds to red-shifted ECL emission wavelength (575 nm). It should be noted that ECL mechanism is different from PL. ECL is surface state luminescence, which electron transfer occurs

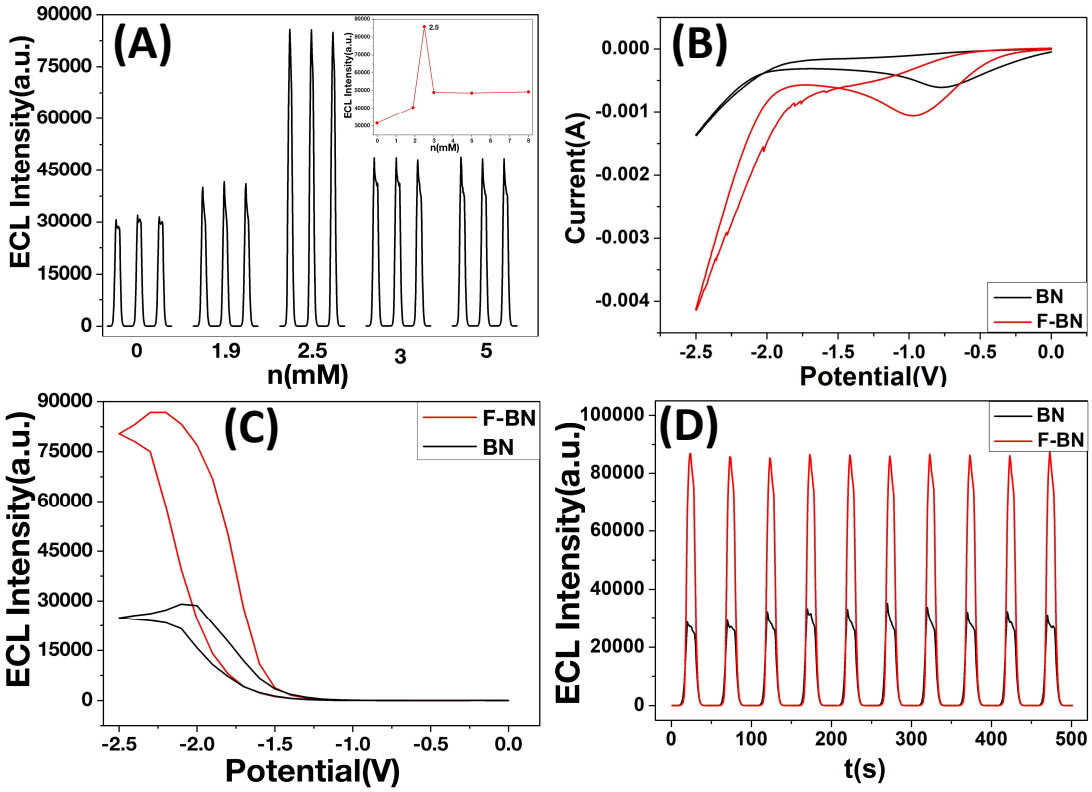

Figure 2. (A) ECL intensity of F-BN QDs synthesized by different amount NH_4F. (B) Cyclic voltammograms of BN QDs/GCE and F-BN QDs/GCE in PBS (pH 7.4) containing 0.1mol/L $K_2S_2O_8$. (C) ECL-potential curves of BN QDs and F-BN QDs in PBS (pH 7.4) containing 0.1mol/L $K_2S_2O_8$. (D) The stability of BN QDs and F-BN QDs.

on the surface of QDs. Surface state ECL energy is less than intrinsic luminescence. Therefore, the ECL peak has the red-shift compared to the PL spectrum. The same phenomenon has also been reported by other related research.[30,31] The polarization character of F-BN QDs ECL was investigated in Figure 1D. With the angle of polarizer changed from 0 to 330°, ECL intensities of F-BN QDs were almost same. It indicated that F-BN QDs generated isotropic ECL without any polarization characteristic.

The ECL behaviors of QDs were studied in PBS (pH=7.4) containing 0.1mol/L $K_2S_2O_8$. The result (Figure 2A) showed the effect of precursor NH_4F in the synthesis of F-BN QDs. The ECL intensity of F-BN QDs increased with the addition of NH_4F and reached maximum as 2.4 times over BN QDs ECL intensity. Cyclic voltammograms (CV) of BN QDs and F-BN QDs were shown in Figure 2B. The reduction potentials of BN QDs and F-BN QDs were -0.80 V and -0.90 V, respectively. BN QDs was slightly easier to be reduced than F-BN QDs. The reduction peak currents of BN QDs and F-BN QDs were observed come to 0.60 mA and 1.03 mA, respectively. It indicated that F-BN QDs can generate more excited states species F-BN QD*, which resulted in the improvement of ECL intensity. Figure 2C showed peak ECL excitation voltages of two kind QDs were both -2.1V. The ECL mechanism of F-BN QDs was shown in Schematic 1A and described as below:

$$\text{F-BN QD} + e^- \rightarrow \text{F-BN QD}^{\bullet-} \quad (1)$$

$$S_2O_8^{2-} + e^- \rightarrow SO_4^{2-} + SO_4^{\bullet-} \quad (2)$$

$$\text{F-BN QD}^{\bullet-} + SO_4^{\bullet-} \rightarrow \text{F-BN QD}^* + SO_4^{2-} \quad (3)$$

$$\text{F-BN QD}^* \rightarrow \text{F-BN QD} + h\nu \quad (4)$$

In ECL reaction, electrons were first injected into the conduction band of QDs. At the same time, a hole was injected into the valence band of QDs by co-reactant ($SO4^{\bullet-}$) which was reduced by the electrode. Subsequent recombination of electrons and holes produced excited states QDs (QDs*), which relaxed to the ground state and ECL emission. The peak ECL potential (-2.1 V) was greater than the negative potential of current (-0.8~-0.9 V). It was due to the interaction of peroxodisulfate or sulfate substance with QD surface which may prevent hole injection.[32] More $SO4^{\bullet-}$ were generated when negative scan potential continues to increase, thereby QDs* increased. The peak potential was exactly the point where concentrations of QDs^- and $SO_4^{\bullet-}$ reached optimal balance and one electron transfer generated QDs*. [33]

The ECL efficiency (Φ_{ECL}) of QDs was calculated according to the below equation:

$$\Phi_{ECL} = \Phi^0_{ECL}(I/I^0)\,(Q^0/Q) \quad (5)$$

In the formula, Φ^0_{ECL} represents ECL efficiency of the standard ($Ru(bpy)_2^{3+}$, 5%). I and I^0 are the integrated ECL intensity of QDs and the standard ($Ru(bpy)_2^{3+}$). Q and Q^0 are

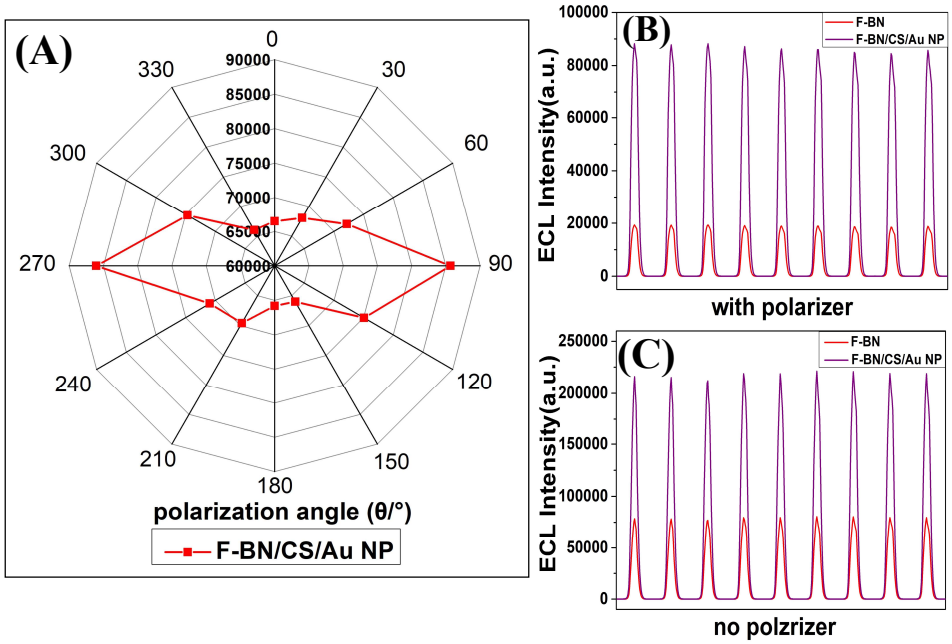

Figure 3. (A) ECL intensity of F-BN QDs with Au NPs at different polarization angle. ECL intensity of F-BN QDs and F-BN QDs with Au NPs when there was a polarizer (B) and no a polarizer (C).

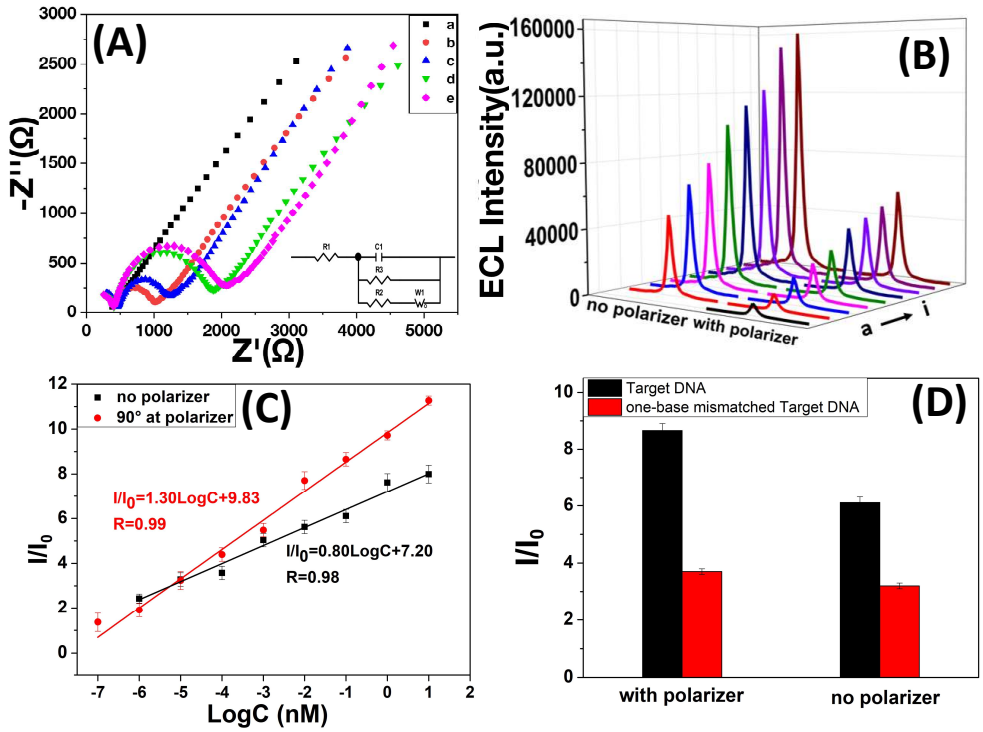

Figure 4. (A) Electrochemical impedance spectroscopy of (a) GCE, (b) GCE/CS, (c) GCE/CS/F-BN QDs/Capture DNA, (d) GCE/CS/F-BN QDs/Capture DNA/Target DNA and (e) GCE /CS /F-BN QDs/Capture DNA/Target DNA/Probe DNA in 0.1 mol/L KCl solution containing 2.5 mmol/L $K_3[Fe(CN)_6]/K_4$ $[Fe(CN)_6]$. (B) The relationship between ECL intensity with different concentrations of K-ras gene (from a to i): 10^{-7}, 10^{-6}, 10^{-5}, 10^{-4}, 10^{-3}, 10^{-2}, 10^{-1}, 1, 10 nmol/L. (C) The corresponding calibration plot for K-ras gene detection. (D) Interference of one-base-mismatched tDNA with ECL response in PBS (pH=7.4) containing 0.1 mol/L $K_2S_2O_8$.

the Faraday charges (in coulombs) of QDs and the standard ($Ru(bpy)_2^{3+}$), respectively. The ECL efficiency of F-BN QDs (Φ_{ECL}=1.83%) increased largely compared with the ECL efficiency of BN QDs (Φ_{ECL}= 0.97%). The stability of QDs (Figure 2D) on glassy carbon electrode (GCE) was investigated by a series of ECL measurements (n=10). The ECL intensity change of F-BN QDs was measured and recorded in Figure S5. There was slight decrease in ECL intensity of F-BN QDs. The results showed that fluorine-doping BN QDs not only improved the ECL intensity (2.4 times), but also provide good stability.

Figure 3A illustrated that ECL signals of F-BN QDs with Au NPs at different polarization angles. Au NPs surface plasmon resonance absorption has a good overlap with the emission spectra of QDs. [34] In the SPC-ECL, the excited state of F-QDs resonated with the electronic oscillation of Au NPs, which caused a significant increase in emission intensity.[35] Furthermore, the isotropic ECL coupled with surface plasmon effect can generate directional emission.[36] The ECL intensities of F-BN QD were analyzed by the polarizing filter and recorded on the radar chart, which clearly showed the intensity changes with polarized angle. It indicated that the SPC effect provided quite different signal amplification at different polarizer angles. As a result, the original isotropic ECL (Figure 1D) of F-BN QDs became polarized ECL (Figure 3A). Based on the SPC-ECL amplification strategy, the maximum ECL intensity reached to 4.6 times of the original signal (Figure 3C) with the polarizing angle (θ = 90°, 270°). In contrast, the total ECL intensity of F-BN QDs only increased 2.6 times over the original isotropic signal (Figure 3B). It was obvious that the polarized ECL system can provide higher resolution.

K-ras gene as called protooncogene, is one of the three main members of the Ras family (H-ras, N-ras and K-ras). K-ras is the most frequently mutated ras subtype and has been shown to mutate in 90% of pancreatic adenocarcinomas, 45% of colorectal cancers and 35% of lung adenocarcinomas.[37-39] K-ras gene quantitative detection is essential in basic research and early cancer diagnosis. A sandwich polarized ECL biosensor based on polarization angle-dependent SPC effect was constructed for K-ras gene detection. As shown in Scheme 1B, a layer of chitosan was first attached to GCE to fix F-BN QDs-capture DNA. We optimized the amount of GA, cross-linking reaction time (Figure S6), and the incubation temperature of K-ras gene (Figure S7). After Probe DNA-Au NPs hybridized with Target DNA, the final SPC-ECL sensing system was formed. The amplified ECL signal of F-BN QDs can be effectively resolved by the polarizer and collected by the detector with photomultiplier tube. As shown in Figure 4A, electrochemical impedance spectroscopy (EIS) showed the change in impedance on the electrode. After modification with chitosan on GCE (curve b), Ret was 252.74Ω. When F-BN QDs-Capture DNA (curve c) were connected to the working electrode, Ret increased to 332.77Ω. Then K-ras gene (curve d) and Probe DNA-Au NPs (curve e) were sequentially captured on the electrode. Due to the insulation and steric hindrance of DNA, Ret of the electrode increased to 597.30Ω and 685.76Ω, respectively. EIS confirmed the successful fabrication of polarized-ECL sensor.

To evaluate analytical performance of polarized-ECL biosensor, the sensor was incubated with different concentrations of K-ras gene. With target DNA concentration increased, more Au NPs were connected to the sensing system. As a result, the ECL gradually increased due to the SPC-ECL effect between Au NPs and QDs (Figure 4B). The calibration curve (Figure 4C) was established based on the changes of I/I_0 with the K-ras gene concentration. I_0 and I represented the ECL intensity of the sensing system without and with K-ras gene, respectively. The result showed that linear range with polarized-ECL intensity was wider (from 0.1 fM to 10nM, R=0.99) than without polarizer (from 1 fM to 10 nM, R=0.98). Furthermore, the detection limit reached to 0.03 fM in polarized-ECL sensing system. We also compared some other methods for K-ras gene detection (Table S2). It indicated that the polarized sensing system had better analysis performance with lower detection limit and higher sensitivity. To evaluate specificity of the biosensor, the responses of 0.1nM K-ras gene and one base mismatched Target DNA were studied under the same condition. The result (Figure 4D) indicated that the same concentration of one-base mismatched DNA did not affect the analytical performance of the polarized biosensor. The proposed ECL biosensor was used to determine K-ras gene in human serum samples. The recovery range (Table S3) was about 93.00-104.0% with relative standard deviation (RSD) as less than 4.63%. The results showed that polarized biosensor for K-ras gene detection was reliable and sensitive.

CONCLUSION

In summary, we constructed a polarized-ECL biosensor based on surface plasmon coupling strategy and F-BN QDs for the first time. Attributed to polarization angle-dependent SPC-ECL, F-BN QDs ECL signal can be enhanced dramatically at a specific polarization angle. ECL signal collection efficiency of SPC-ECL sensing system can be improved with the assistance of a polarizer. Based on the polarized-ECL amplification strategy, a sandwich-type polarized-ECL biosensor was designed for K-ras gene detection. There are many unresolved issues in the polarized ECL research. For example, the relationship between polarization angle and the material needs to be investigated. The weak polarized ECL can cause low sensitivity in the sensing application. With new nanomaterials developments and novel analytical instruments design, the polarized-ECL biosensor can promote the development of bioanalysis and open a new way to the polarization angle-resolved sensing research in the future.

ASSOCIATED CONTENT

Supporting Information paragraph

The Supporting Information is available free of charge on the ACS Publications website.

Chemicals and apparatus, Synthesis of BN QDs, TEM image of F-BN QDs (Figure S1), XPS survey spectrum of F-BN QDs (Figure S2), UV-vis spectra of BN QDs and F-BN QDs (Figure S3), ECL spectrum and PL spectrum of BN QDs (Figure S4), ECL intensity of QDs in 30 days (Figure

S5), volume and reaction time of Glutaraldehyde (Figure S6), ECL intensity and K-ras gene incubation temperature (Figure S7), sequences of the used oligonucleotides in present work (Table S1), comparison of other methods with this work (Table S2), and detection of target DNA in human serum (Table S3). (PDF)

AUTHOR INFORMATION

Corresponding Author

* Tel.: +86-431-85168352. E-mail: qma@jlu.edu.cn
ORCID
Qiang Ma: 0000-0003-4841-5005

Notes

The authors declare no competing financial interest

ACKNOWLEDGMENTS

The authors gratefully acknowledge financial support from Youth Science Fund of Jilin Province (20140520081JH) and "Thirteenth Five Year" Project of the Science and Technology Research in the Education Department of Jilin Province, China.

REFERENCES

(1) Pyati, R.; Richter, M. M. ECL—Electrochemical luminescence. Annu. Rep. Prog. Chem., Sect. C. 2007, 103, 12–78.
(2) Hu, L.; Xu, G. Applications and trends in electrochemiluminescence. Chem. Soc. Rev. 2010, 39, 3275–3304.
(3) Li, L.; Chen, Y.; Zhu, J. Recent Advances in Electrochemiluminescence Analysis. Anal. Chem. 2017, 89, 358−371.
(4) Lei, J.; Ju, H. Fundamentals and bioanalytical applications of functional quantum dots as electrogenerated emitters of chemiluminescence. Trends Anal. Chem. 2011, 30, 1351-1359.
(5) Zhang, J.; Kang, T.; Hao, Y.; Lu, L.; Cheng, S. Electrochemiluminescent immunosensor based on CdS quantum dots for ultrasensitive detection of microcystin-LR. Sens. Actuators, B. 2015, 214, 117–123.
(6) Han, S.; Gao Y.; Li, L.; Lu, B.; Zou, Y,; Zhang, L.; Zhang, J. Synergistic Enhancement Effects of Carbon Quantum Dots and Au Nanoclusters for Cathodic ECL and Non-enzyme Detections of Glucose. Electroanaly. 2020, 32, 1–6.
(7) Jie, G.; Zhou, Q.; Jie, G. Graphene quantum dots-based electrochemiluminescence detection of DNA using multiple cycling amplification strategy. Talanta. 2019, 194, 658–663.
(8) Zhao, W.; Kang, T.; Xu, Y.; Zhang, X.; Liu, H.; Ming, A.; Lu, L.; Cheng, S.; Wei, F. Electrochemiluminescence solid-state imprinted sensor based on graphene/CdTe@ZnS quantum dots as luminescent probes for low-cost ultrasensing of diethylstilbestrol. Sens. Actuators B Chem. 2020, 306, 127563.
(9) Li, Y.; Chu, Y.; Li, Y.; Ma, C.; Li, L. A novel electrochemiluminescence biosensor: Inorganic-organic nanocomposite and $ZnCo_2O_4$ as the efficient emitter and accelerator. Sens. Actuators B Chem. 2020, 303, 127222.
(10) Li, P.; Yu, J.; Zhao, K.; Deng, A.; Li, J. Efficient enhancement of electrochemiluminescence from tin disulfide quantum dots by hollow titanium dioxide spherical shell for highly sensitive detection of chloramphenicol. Biosens. Bioelectron. 2020, 147, 111790.
(11) Ding, H.; Guo, W.; Su, B. Imaging Cell-Matrix Adhesions and Collective Migration of Living Cells by Electrochemiluminescence Microscopy. Angew. Chem. Int. Ed. 2020, 59, 449–456.
(12) Zhang, H.; Gao, W.; Liu, Y.; Sun, Y.; Jiang, Y.; Zhang, S. Electrochemiluminescence-Microscopy for microRNA Imaging in Single Cancer Cell Combined with Chemotherapy-Photothermal Therapy. Anal. Chem. 2019, 91, 12581−12586.
(13) Zhang, J.; Jin, R.; Jiang, D.; Chen, H. Electrochemiluminescence-Based Capacitance Microscopy for Label-Free Imaging of Antigens on the Cellular Plasma Membrane. J. Am. Chem. Soc. 2019, 141, 10294−10299.
(14) Liu, G.; Jin, B.; Ma, C.; Chen, Z.; Zhu, J. Potential-Resolved Electrochemiluminescence Nanoprobes for Visual Apoptosis Evaluation at Single-Cell Level. Anal. Chem. 2019, 91, 6363−6370.
(15) Zhu, L.; Ye, J.; Yan, M.; Zhu, Q.; Yang, X. A wavelength-resolved electrochemiluminescence resonance energy transfer ratiometric immunosensor for detection of cardiac troponin I. Analyst. 2019, 144, 6554–6560.
(16) Lv, Y.; Zhou, Z.; Shen, Y.; Zhou, Q.; Ji, J.; Liu, S.; Zhang Y. Coupled Fluorometer-Potentiostat System and Metal-Free Monochromatic Luminophores for High-Resolution Wavelength-Resolved Electrochemiluminescent Multiplex Bioassay. ACS Sens. 2018, 3, 1362−1367.
(17) Cao, J.; Fu, X.; Liu, F.; Ren, S.; Liu, Y. Reduced graphene oxide-gold nanoparticles-catalase-based dual signal amplification strategy in a spatial-resolved ratiometric electrochemiluminescence immunoassayAnalyst. 2020, 145, 91–96.
(18) Wang, Y.; Zhang, Y.; Sha, H.; Xiong, X.; Jia, N. Design and Biosensing of a Ratiometric Electrochemiluminescence Resonance Energy Transfer Aptasensor between a g-C_3N_4 Nanosheet and Ru@MOF for Amyloid-β Protein. ACS Appl. Mater. Interfaces. 2019, 11, 36299−36306.
(19) Li, Y.; Wang, L.; Ding, C.; Luo, X. Highly selective ratiometric electrogenerated chemiluminescence assay of DNA methyltransferase activity via polyaniline and anti-fouling peptide modified electrode. Biosens. Bioelectron. 2019, 142, 111553.
(20) Zinna, F.; Voci, S.; Arrico, L.; Brun, E.; Homberg, A.; Bouffier, L.; Funaioli, T.; Lacour, J.; Sojic, N.; Bari, L. D. Circularly-Polarized Electrochemiluminescence from a Chiral Bispyrene Organic Macrocycle. Angew. Chem. Int. Ed. 2019, 58, 6952–6956.
(21) Liu, Y.; Wang, M,; Nie, Y.; Zhang, Q.; Ma, Q. Sulfur Regulated Boron Nitride Quantum Dots Electrochemiluminescence with Amplified Surface Plasmon Coupling Strategy for BRAF Gene Detection. Anal. Chem. 2019, 91, 6250−625.
(22) Aslan, K.; Geddes, C. D. Metal-enhanced chemiluminescence: advanced chemiluminescence concepts for the 21st century. Chem. Soc. Rev. 2009, 38, 2556–2564.
(23) Park, J.; Shumaker-Parry J. Structural Study of Citrate Layers on Gold Nanoparticles: Role of Intermolecular Interactions in Stabilizing Nanoparticles. J. Am. Chem. Soc. 2014, 136, 1907−1921.
(24) Du, M.; Li, X.; Wang, A.; Wu, Y. ; Hao, X.; Zhao, M. One-Step Exfoliation and Fluorination of Boron Nitride Nanosheets and a Study of Their Magnetic Properties. Angew. Chem. Int. Ed. 2014, 53, 3645–3649.
(25) Tang, C.; Bando, Y.; Huang, Y.; Yue, S.; Gu, C.; Xu, F.; Golberg, D. Fluorination and Electrical Conductivity of BN Nanotubes. J. Am. Chem. Soc. 2005, 127, 6552-6553.
(26) Venkateswarlu, G.; Madhu, D.; Rani, J. V. An effective performance of F-Doped hexagonal boron nitride nanosheets as cathode material in magnesium battery. Mater. Chem. Phys. 2019, 226 ,356–361.
(27) Peng, D.; Jiang, W.; Li, F.; Zhang, L.; Liang, R.; Qiu, J. One-Pot Synthesis of Boron Carbon Nitride Nanosheets for Facile and Efficient Heavy Metal Ions Removal. ACS Sustainable Chem. Eng. 2018, 6, 11685−11694.

(28) Tang, C.; Bando, Y.; Huang, Y.; Yue, S.; Gu, C.; Xu, F.; Golberg, D. Fluorination and Electrical Conductivity of BN Nanotubes. J. Am. Chem. Soc. 2005, 127, 6552-6553.
(29) Shen, T.; Liu, S.; Yan, W.; Wang, J. Highly efficient preparation of hexagonal boron nitride by direct microwave heating for dye removal. J Mater Sci. 2019, 54, 8852–8859.
(30) Ding, Z.; Quinn, B. M. ; Haram, S. K.; Pell, L. E.; Korgel, B. A.; Bard, A. Electrochemistry and Electrogenerated Chemiluminescence from Silicon Nanocrystal Quantum Dots. Science. 2002, 296, 1293-1297.
(31) Myung, N.; Bae, Y.; Bard, A. J. Effect of surface passivation on the electrogenerated chemiluminescence of CdSe/ZnSe nanocrystals. Nano Lett. 2003, 3, 1053-1055.
(32) Bao, L.; Sun, LF.; Zhang, ZL.; Jiang, P.; Wise, FW.; Abruna, HD.; Pang, DW. Energy-Level-Related Response of Cathodic Electrogenerated-Chemiluminescence of Self-Assembled CdSe/ZnS Quantum Dot Films. J Phys Chem C. 2011, 115, 18822-18828.
(33) Zhang, RZ.; Adsetts, JR .; Nie, YT.; Sun, XH.; Ding, ZF. Electrochemiluminescence of nitrogen- and sulfur-doped graphene quantum dots. CARBON. 2018, 129, 45-53.
(34) Chen, HL.; Cheng, HC.; Ko, TS. ; Chuang, SY.; Chu, TC. Characterizing optical properties of self-assembled gold nanoparticles for surface plasmon resonance device applications. Jpn J Appl Phys. 2006, 45, 6984-6986.
(35) Zhang, Q.; Liu, Y.; Nie, Y.; Liu, Y.; Ma, Q. Wavelength-Dependent Surface Plasmon Coupling Electrochemiluminescence Biosensor Based on Sulfur-Doped Carbon Nitride Quantum Dots for K RAS Gene DetectionAnal. Chem. 2019, 91, 13780−13786.
(36) Zhang, J.; Gryczynski, Z.; Lakowicz, J. R. First observation of surface plasmon-coupled electrochemiluminescence. Chemical Physics Letters. 2004, 393, 483–487.
(37) Adjei, A. A. Blocking Oncogenic Ras Signaling for Cancer Therapy. J. Natl. Cancer Inst. 2001, 93, 1062-1074.
(38) Downward, J. Targeting RAS signalling pathways in cancer therapy. Nature Reviews Cancer. 2003, 3, 11-22.
(39) Wang, Y.; Kaiser, C. E.; Frett, B.; Li, H. Targeting Mutant KRAS for Anticancer Therapeutics: A Review of Novel Small Molecule Modulators. J. Med. Chem. 2013, 56, 5219−5230.

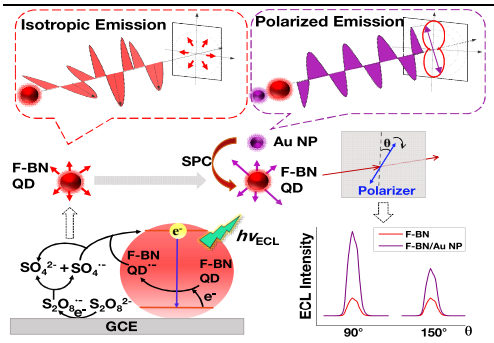
Isotropic Emission
Polarized Emission
F-BN QD
SPC
Au NP
F-BN QD
Polarizer
θ
F-BN
F-BN/Au NP
ECL Intensity
90°
150°
θ
hv_{ECL}
$SO_4^{2-} + SO_4^{\cdot-}$
F-BN QD$^{\cdot-}$
F-BN QD
e$^-$
$S_2O_8^{\cdot-}$ $S_2O_8^{2-}$
GCE